



Study of Mach Number Effect for 2D Co-Flow Jet Airfoil at Cruise Conditions

Yang Wang * Gecheng Zha †
Dept. of Mechanical and Aerospace Engineering
University of Miami, Coral Gables, Florida 33124
E-mail: gzha@miami.edu

Abstract

This paper studies the Mach number effect on cruise performance for a 2D Co-Flow Jet (CFJ) airfoil at freestream Mach number of 0.15, 0.30, 0.46 and 0.5. The optimized 2D CFJ airfoil, CFJ6421-SST150-SUC247-INJ117 is redesigned by enlarging the size of the injection and suction slot from the CFJ airfoil previously designed by Lefebvre and Zha. The results show that the best CFJ airfoil corrected aerodynamic efficiency $((C_L/C_D)_c)$ occurs at M_∞ of 0.30, which produces a $(C_L/C_D)_c$ of 81.04 at C_μ of 0.03 and AoA of 6° . The case at M_∞ of 0.30 has higher compressibility than that at M_∞ of 0.15, but is still far from the sonic speed. The favorable conditions hence provide the optimum aerodynamic efficiency. At the same C_μ and AoA , the maximum Mach number on the CFJ airfoil suction surface at M_∞ of 0.15, 0.30, 0.46, 0.50 is 0.264, 0.558, 1.025 and 1.289 respectively. For the case of M_∞ of 0.50, the flow becomes transonic. As the M_∞ increases, the C_L is also increased due to the stronger compressibility effect that creates a greater suction effect. At M_∞ of 0.46, which is the critical Mach number for the airfoil at AoA of 6° , the corrected aerodynamic efficiency is still very good. But when the M_∞ is increased to 0.5, the optimum aerodynamic efficiency occurs at a lower AoA and C_μ with $AoA = 2^\circ$ and $C_\mu = 0.01$. Under this condition, the flow remain subsonic without shock wave. For the optimum cruise condition with the Mach number varying from 0.15 to 0.5, the ratio of the injection jet velocity to the freestream velocity is varied from 1.24 to 0.68, and the total pressure ratio between the injection and suction slot is from 1.02 to 1.20. The low CFJ jet velocity is beneficial to reduce the noise and the low total pressure ratio is beneficial to achieve the low power requirement at cruise. Comparing the optimum efficiency point of the baseline NACA 6421 airfoil and CFJ airfoil, the CFJ airfoil improves the lift coefficient by 30%. The aerodynamic efficiency is improved by 60% or more (under 100% pump efficiency) and 40% or more (under 70% pump efficiency).

This paper also studies two control laws for cruise control of the CFJ airfoil when the AoA varies: One is to achieve constant injection momentum coefficient, the other is to achieve constant injection total pressure. The latter is preferred for its easier sensor measurement, higher airfoil efficiency, and higher stall AoA . The numerical simulations employ the intensively validated in house FASIP CFD code, which utilizes a 3D RANS solver with Spalart-Allmaras (S-A) turbulence model, 3rd order WENO scheme for the inviscid fluxes, and 2nd order central differencing for the viscous terms.

Nomenclature

| | |
|------------|-----------------|
| <i>CFJ</i> | Co-flow jet |
| <i>AoA</i> | Angle of attack |
| <i>LE</i> | Leading Edge |

* Graduate Student

† Professor, ASME Fellow, AIAA associate Fellow

| | |
|---------------|---|
| TE | Trailing Edge |
| S | Planform area |
| c | Airfoil chord |
| U | Flow velocity |
| q | Dynamic pressure $0.5 \rho U^2$ |
| p | Static pressure |
| η | Pump efficiency |
| ρ | Air density |
| \dot{m} | Mass flow |
| M | Mach number |
| ω | Pitching Moment |
| P | Pumping power |
| ∞ | Free stream conditions |
| j | Jet conditions |
| C_L | Lift coefficient $L/(q_\infty S)$ |
| C_D | Drag coefficient $D/(q_\infty S)$ |
| C_M | Moment coefficient |
| C_μ | Jet momentum coef. $\dot{m}_j U_j/(q_\infty S)$ |
| $(C_L/C_D)_c$ | CFJ airfoil corrected aerodynamic efficiency $L/(D + P/V_\infty)$ |
| P_c | Power coefficient $L/(q_\infty S V_\infty)$ |
| PR | Total pressure ratio between injection and suction |
| M_{i_s} | Isentropic Mach Number |
| M_∞ | Freestream Mach Number |
| P_{tinj} | Total injection pressure |
| P_{tsuc} | Total suction pressure |
| V_{inj} | Normalized injection velocity |

1 Introduction

High cruise efficiency is crucial to minimize the energy consumption of airliners. This is particularly important for electric aircraft development to extend range and increase payload with the current limited battery energy density. However, increasing aircraft aerodynamic efficiency at cruise condition is very challenging because the flow condition is usually very benign at a low angle of attack. Most of the efforts to increase cruise efficiency in the past few decades are focused on 3D combination, including winglet, wing body combination, flying wing, boundary layer ingestion with integrated propulsion system and fuselage, distributed propulsion, etc. Few efforts are focused on improving the airfoil performance at cruise condition since they are considered mature with little room to improve.

Recently, the Co-Flow Jet (CFJ) flow control airfoil developed by Zha et al. [1, 2, 3, 4, 5, 6, 7, 8, 9, 10, 11, 12] provides a promising concept to improve the cruise efficiency. In a CFJ airfoil, an injection slot near the leading edge (LE) and a suction slot near the trailing edge (TE) on the airfoil suction surface are created. As shown in Fig. 1, a small amount of mass flow is drawn into the suction duct, pressurized and energized by the micro compressor, and then injected near the LE tangentially to the main flow via an injection duct. The whole process does not add any mass flow to the system and hence is a zero-net-mass-flux (ZNMF) flow control. The CFJ airfoil is demonstrated to achieve radical lift augmentation, stall margin increase, drag reduction and moderate nose-down

moment for stationary and pitching airfoils.

The CFJ airfoil has a unique low energy expenditure mechanism, because the jet gets injected at the leading edge peak suction location, where the main flow pressure is the lowest and makes it easy to inject the flow, and it gets sucked at the trailing edge, where the main flow pressure is the highest and makes it easy to draw the flow. The low energy expenditure is a key factor enabling the CFJ airfoil to achieve ultra-high cruise efficiency [13] at low AoA when the flow is benign.

Since aircraft operate at different cruise speeds, a question that needs to ask is how freestream Mach number affects the CFJ airfoil corrected efficiency. The purpose of this paper is to study this problem by simulating 2D CFJ airfoils with different M_∞ at varying jet injection momentum coefficient and AoA . For a CFJ airplane at cruise, the AoA will vary due to disturbance. A control target, or control law, needs to be defined for the micro-compressors. Two control laws are studied: one is to have constant injection momentum coefficient, the other is to have a constant injection total pressure. The jet momentum coefficient is usually used to study the CFJ airfoil performance in laboratory. The total pressure is much easier to control for its simplicity of measurement. Furthermore, the present study discovers that a constant total pressure gives higher efficiency and larger stall AoA . The Mach number studied in this paper is limited to 0.5 to avoid going into transonic regime, which needs CFJ super-critical airfoil and the cruise performance is studied in [14].

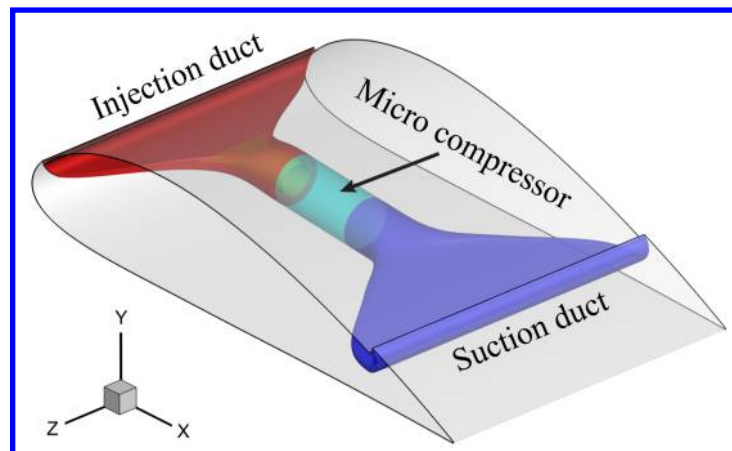


Figure 1: Schematic plot of a typical CFJ airfoil.

2 Methodology

2.1 Lift and Drag Calculation

The momentum and pressure at the injection and suction slots produce a reactionary force, which is automatically measured by the force balance in wind tunnel testing. However, for CFD simulation, the full reactionary force needs to be included. Using control volume analysis as shown in Fig. 2, the reactionary force can be calculated using the flow parameters at the injection and suction slot opening surfaces. Zha et al. [2] give the following formulations to calculate the lift and drag due to the jet reactionary force for a CFJ airfoil. By considering the effects of injection and suction jets on the CFJ airfoil, the expressions for these reactionary forces are given as :

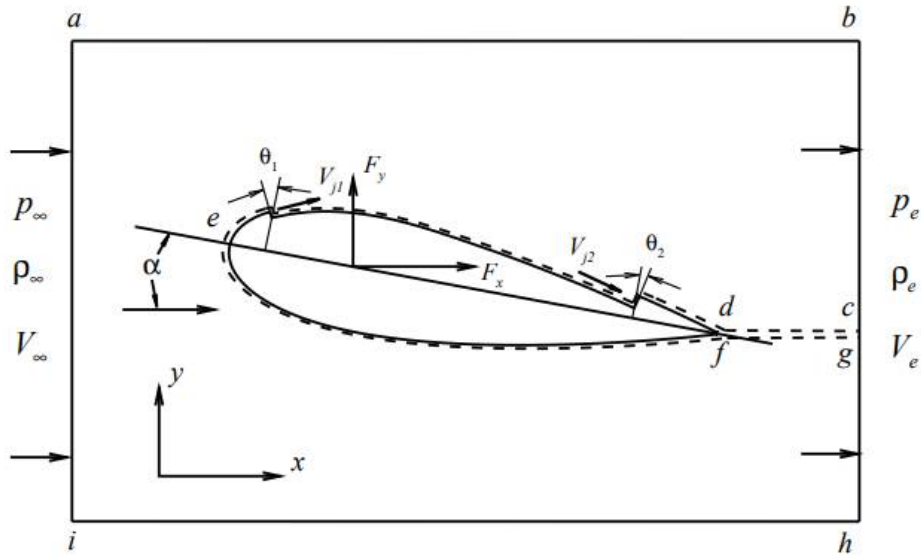


Figure 2: The control volume for a CFJ airfoil.

$$F_{x_{cfj}} = (\dot{m}_j V_{j1} + p_{j1} A_{j1}) * \cos(\theta_1 - \alpha) - (\dot{m}_j V_{j2} + p_{j2} A_{j2}) * \cos(\theta_2 + \alpha) \quad (1)$$

$$F_{y_{cfj}} = (\dot{m}_{j1} V_{j1} + p_{j1} A_{j1}) * \sin(\theta_1 - \alpha) + (\dot{m}_{j2} V_{j2} + p_{j2} A_{j2}) * \sin(\theta_2 + \alpha) \quad (2)$$

where the subscripts 1 and 2 stand for the injection and suction respectively, and θ_1 and θ_2 are the angles between the injection and suction slot's surface and a line normal to the airfoil chord. α is the angle of attack.

The total lift and drag on the airfoil can then be expressed as:

$$D = R'_x - F_{x_{cfj}} \quad (3)$$

$$L = R'_y - F_{y_{cfj}} \quad (4)$$

where R'_x and R'_y are the surface integral of pressure and shear stress in x (drag) and y (lift) direction excluding the internal ducts of injection and suction. For CFJ wing simulations, the total lift and drag are calculated by integrating Eq. (3) and Eq. (4) in the spanwise direction.

2.2 Jet Momentum Coefficient

The jet momentum coefficient C_μ is a parameter used to quantify the jet intensity. It is defined as:

$$C_\mu = \frac{\dot{m} V_j}{\frac{1}{2} \rho_\infty V_\infty^2 S} \quad (5)$$

where \dot{m} is the injection mass flow, V_j is the mass-averaged injection velocity, ρ_∞ and V_∞ denote the free stream density and velocity, and S is the planform area.

2.3 Power Coefficient

CFJ is implemented by mounting a pumping system inside the wing that withdraws air from the suction slot and blows it into the injection slot. The power consumption is determined by the jet mass flow and total enthalpy change as the following:

$$P = \dot{m}(H_{t1} - H_{t2}) \quad (6)$$

where H_{t1} and H_{t2} are the mass-averaged total enthalpy in the injection cavity and suction cavity respectively, P is the Power required by the pump and \dot{m} the jet mass flow rate. Introducing P_{t1} and P_{t2} the mass-averaged total pressure in the injection and suction cavity respectively, the pump efficiency η , and the total pressure ratio of the pump $\Gamma = \frac{P_{t1}}{P_{t2}}$, the power consumption is expressed as:

$$P = \frac{\dot{m}C_p T_{t2}}{\eta} (\Gamma^{\frac{\gamma-1}{\gamma}} - 1) \quad (7)$$

where γ is the specific heat ratio equal to 1.4 for air. The power coefficient is expressed as:

$$P_c = \frac{P}{\frac{1}{2}\rho_\infty V_\infty^3 S} \quad (8)$$

2.4 Corrected Aerodynamic Efficiency

The conventional wing aerodynamic efficiency is defined as:

$$\frac{L}{D} \quad (9)$$

For the CFJ wing, the ratio above still represents the pure aerodynamic relationship between lift and drag. However since CFJ active flow control consumes energy, the ratio above is modified to take into account the energy consumption of the pump. The formulation of the corrected aerodynamic efficiency for CFJ wings is:

$$\left(\frac{L}{D}\right)_c = \frac{C_L}{C_D + P_c} \quad (10)$$

where V_∞ is the free stream velocity, P is the pumping power, and L and D are the lift and drag generated by the CFJ wing. The formulation above converts the power consumed by the CFJ into a force $\frac{P}{V_\infty}$ which is added to the aerodynamic drag D . If the pumping power is set to 0, this formulation returns to the aerodynamic efficiency of a conventional wing.

2.5 Aircraft Productivity

To compare aircraft that have the same ratio of initial weight to final weight with the same engine fuel consumption or battery energy density, the productivity efficiency C_L^2/C_D is introduced to measure the productivity of an airplane represented by its range multiplied by its weight [15].

The productivity efficiency $C_L^2/C_D = C_L(C_L/C_D)$ is a more comprehensive parameter than the conventional aerodynamic efficiency C_L/C_D to measure the merit of an airplane aerodynamic design for cruise performance. The former includes not only the information of C_L/C_D , but also the information of the aircraft weight C_L . For example, for two airplane designs having the same C_L/C_D with one C_L twice larger than the other, if the wing sizes are the same, one airplane will be able to carry twice more weight than the other with productivity and wing loading increased by 100%. Such a large difference is not reflected by C_L/C_D , but very well reflected by C_L^2/C_D .

The definition of C_L/C_D in general is a suitable measure of merit for conventional aircraft design. This is because at a certain Mach number regime, the maximum C_L/C_D is usually achieved at low angle of attack within the drag bucket and is more or less the same for different airfoil designs. In other words, for the same optimum C_L/C_D , the C_L is about the same. A typical C_L for subsonic airfoil is about 0.4 and for transonic airfoil is about 0.7.

For CFJ airfoil, the minimum CFJ pumping power occurs at a fairly high AoA [7, 16]. With the augmentation of CFJ, the subsonic cruise lift coefficient of a CFJ airfoil is typically 2 to 3 times higher than the conventional airfoil with about the same $(C_L/C_D)_c$ [12]. Such a high lift coefficient is unattainable for conventional airfoil since they would be either stalled or near stalled with very high drag. Hence for CFJ aircraft design, the productivity efficiency $C_L^2/C_D = C_L(C_L/C_D)$ is more informative to be used to reflect the aerodynamic performance. The corrected productivity efficiency for CFJ airfoils is $(C_L^2/C_D)_c = C_L^2/(C_D + P_c)$.

2.6 CFD Simulation Setup

The FASIP (Flow-Acoustics-Structure Interaction Package) CFD code is used to conduct the numerical simulation. The 3D Reynolds Averaged Navier-Stokes (RANS) equations with one-equation Spalart-Allmaras [17] turbulence model is used. A 3rd order WENO scheme for the inviscid flux [18, 19, 20, 21, 22, 23] and a 2nd order central differencing for the viscous terms [18, 22] are employed to discretize the Navier-Stokes equations. The low diffusion E-CUSP scheme used as the approximate Riemann solver suggested by Zha et al [19] is utilized with the WENO scheme to evaluate the inviscid fluxes. Implicit time marching method using Gauss-Seidel line relaxation is used to achieve a fast convergence rate [24]. Parallel computing is implemented to save wall clock simulation time [25].

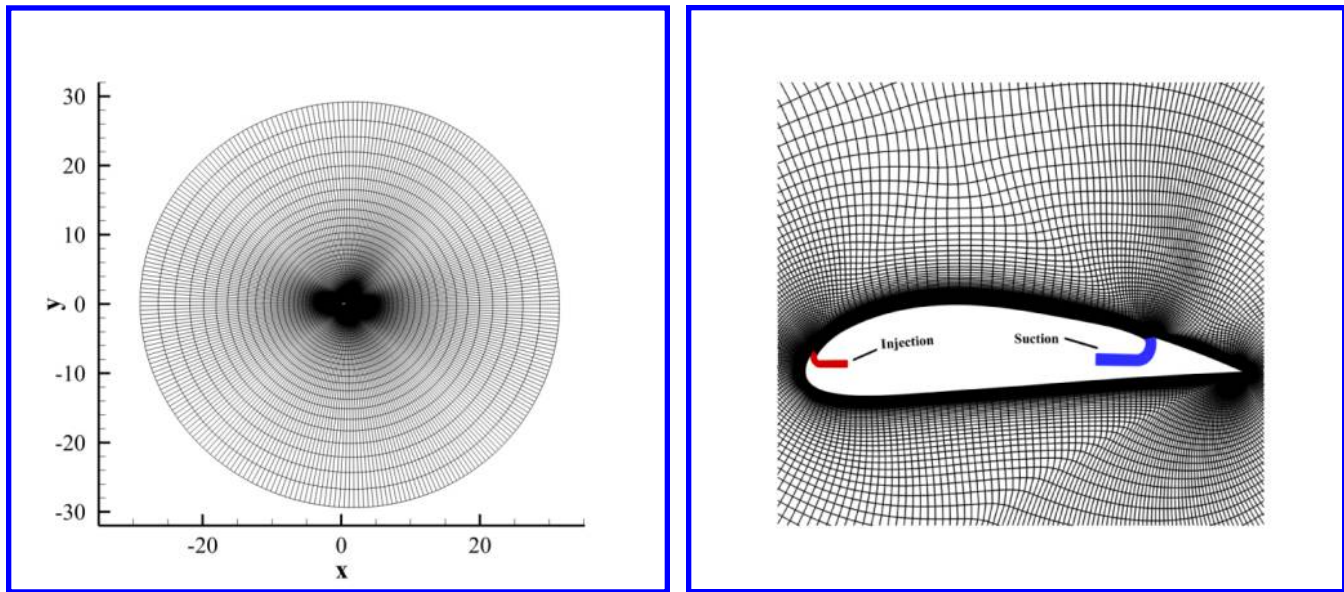


Figure 3: Computational mesh used in the current work.

2.7 Boundary Conditions

The 3rd order accuracy no slip condition is enforced on the solid surface with the wall treatment suggested in [26] to achieve the flux conservation on the wall. The computational mesh is shown in Fig. 3. The ducts geometries are predetermined according to our previous designs. Total pressure, total temperature and flow angles are specified at the injection duct inlet, as well as the upstream portion of the far field. Constant static pressure is applied at the suction duct outlet as well as the downstream portion of the far field. The total mesh size is 47,200 points, split into 10 domains for the parallel computation. The first grid point on the wing surface is placed at $y^+ \approx 1$. This mesh size is same as the mesh size used in Lefebvre's study[12].

3 Airfoil Geometry Parameters

Table. 1 gives the detailed parameters of two different designs of CFJ6421 airfoils with the injection and suction slot size normalized by airfoil chord length (C). The CFJ6421-SST150-SUC247-INJ117 airfoil is optimized by enlarging the injection and suction size based on the CFJ6421-SST150-SUC133-INJ065 which is designed by Lefebvre and Zha[12]. The CFJ6421-SST150-SUC247-INJ117 airfoil has a larger injection slot size of $1.17\%C$ and suction slot size of 2.47% . The suction surface translation (SST) of $1.50\%C$ is the same as that of CFJ6421-SST150-SUC133-INJ065 airfoil. Both airfoils are developed based on the NACA 6421 airfoil. For simplicity of description, the CFJ6421-SST150-SUC133-INJ065 airfoil and CFJ6421-SST150-SUC247-INJ117 airfoil are named CFJ 1 and CFJ 2 airfoil. The CFJ 2 airfoil has the injection and suction slot size larger than those of the CFJ 1 airfoil by 80% and 86% respectively.

Table 1: Airfoil geometry parameters

| Airfoil | SST (%C) | INJ (%C) | SUC (%C) |
|--------------------------------------|----------|----------|----------|
| CFJ6421-SST150-SUC133-INJ065 (CFJ 1) | 1.50 | 0.65 | 1.33 |
| CFJ6421-SST150-SUC247-INJ117 (CFJ 2) | 1.50 | 1.17 | 2.47 |
| NACA6421 (Baseline airfoil) | N/A | N/A | N/A |

4 Simulated Cases

The CFJ 2 airfoil is used for the study of freestream Mach Number effect. Table. 2 lists all the freestream conditions and the CFJ momentum coefficients that are studied. Since the focus is on the cruise performance, the AoA is limited to low value of $0^\circ - 14^\circ$.

Table 2: Simulation cases used in the current work

| Cases | M_∞ | AoA | C_μ |
|-------|------------|--------------------|-------------|
| 1 | 0.15 | $0^\circ-14^\circ$ | 0.01 - 0.05 |
| 2 | 0.30 | $0^\circ-14^\circ$ | 0.01 - 0.05 |
| 3 | 0.46 | $0^\circ-14^\circ$ | 0.01 - 0.05 |
| 4 | 0.50 | $0^\circ-14^\circ$ | 0.01 - 0.05 |

5 Performance of CFJ Airfoils

Table. 3 lists the airfoil optimum aerodynamic efficiency at different freestream Mach number. The CFJ power efficiency is assumed as 100%. As shown in Fig. 4 (a), for M_∞ of 0.15, the optimum $(C_L/C_D)_c$ is 74.094 at C_μ 0.03 and AoA of 6° . At M_∞ of 0.30, the optimum $(C_L/C_D)_c$ is 81.04 at the same C_μ and AoA (see Fig. 4 (b)). At M_∞ of 0.46, the optimum corrected aerodynamic efficiency drops slightly. However, at M_∞ of 0.50, the optimum $(C_L/C_D)_c$ drops slightly to 76.09 at C_μ 0.01 and at AoA of 2° , but still higher than that of Mach 0.15.

Table 3: Airfoil performance at different M_∞ for CFJ 2 airfoil with 100% pump efficiency.

| M_∞ | C_L | C_L/C_D | $(C_L/C_D)_c$ | $(C_L^2/C_D)_c$ | AoA | C_μ | Pc | η |
|------------|--------|-----------|---------------|-----------------|-----------|---------|---------|--------|
| 0.15 | 1.4145 | 107.799 | 74.094 | 104.804 | 6° | 0.03 | 0.00597 | 100% |
| 0.30 | 1.4949 | 120.883 | 81.035 | 121.137 | 6° | 0.03 | 0.00608 | 100% |
| 0.46 | 1.6933 | 132.489 | 77.092 | 130.541 | 6° | 0.03 | 0.00918 | 100% |
| 0.50 | 1.0758 | 101.081 | 76.087 | 81.853 | 2° | 0.01 | 0.00350 | 100% |

Table. 4 lists the results when assuming the micro-compressor efficiency as 70%. Both the aerodynamic efficiency and productivity efficiency are decreased, but still at very high level.

Table 4: Airfoil performance at different M_∞ for CFJ 2 airfoil with 70% pump efficiency.

| M_∞ | C_L | C_L/C_D | $(C_L/C_D)_c$ | $(C_L^2/C_D)_c$ | AoA | C_μ | P_c | η |
|------------|--------|-----------|---------------|-----------------|-----|---------|---------|--------|
| 0.15 | 1.4145 | 107.799 | 65.338 | 92.420 | 6° | 0.03 | 0.00853 | 70% |
| 0.30 | 1.4949 | 120.883 | 71.004 | 106.142 | 6° | 0.03 | 0.00869 | 70% |
| 0.46 | 1.6933 | 132.489 | 65.377 | 110.704 | 6° | 0.03 | 0.01312 | 70% |
| 0.50 | 1.0758 | 101.081 | 68.797 | 74.010 | 2° | 0.01 | 0.00350 | 70% |

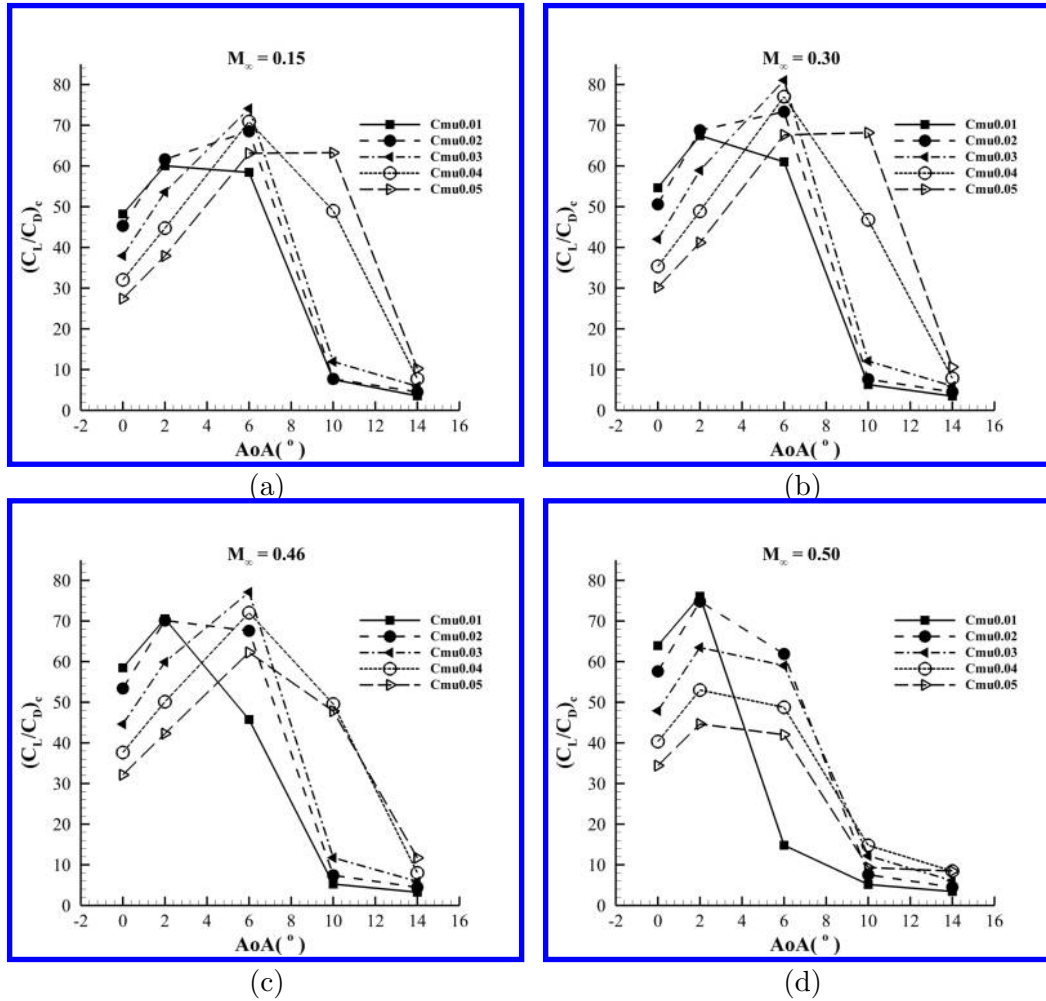


Figure 4: CFJ airfoil corrected efficiency for CFJ 2 airfoil at M_∞ of 0.15, 0.30, 0.46 and 0.50.

For comparison reference, Table. 5 and Table. 7 list the airfoil optimum aerodynamic efficiency at different freestream Mach number for the CFJ 1 airfoil and the baseline NACA 6421 airfoil. Comparing Table. 5 and Table. 7, the CFJ 1 airfoil has the cruise lift coefficient about 20% - 30% higher than that of the baseline airfoil. At the same time, the aerodynamic efficiency is increased by about 50%. Comparing Table. 3 and Table. 5, the CFJ 2 airfoil with larger injection and suction slot, which further increases the lift coefficient and aerodynamic efficiency by about 5% or more.

Table 5: Airfoil performance at different M_∞ for CFJ 1 airfoil with 100% pump efficiency.

| M_∞ | C_L | C_L/C_D | $(C_L/C_D)_c$ | $(C_L^2/C_D)_c$ | AoA | C_μ | Pc | η |
|------------|--------|-----------|---------------|-----------------|-------|---------|---------|--------|
| 0.15 | 1.3203 | 83.975 | 70.716 | 93.364 | 6° | 0.02 | 0.00295 | 100% |
| 0.30 | 1.3856 | 90.546 | 76.179 | 105.550 | 6° | 0.02 | 0.00289 | 100% |
| 0.46 | 1.6724 | 139.128 | 76.929 | 128.659 | 6° | 0.03 | 0.00972 | 100% |
| 0.50 | 1.0411 | 86.274 | 69.041 | 71.876 | 2° | 0.01 | 100% | |

Table 6: Airfoil performance at different M_∞ for CFJ 1 airfoil with 70% pump efficiency.

| M_∞ | C_L | C_L/C_D | $(C_L/C_D)_c$ | $(C_L^2/C_D)_c$ | AoA | C_μ | Pc | η |
|------------|--------|-----------|---------------|-----------------|-------|---------|---------|--------|
| 0.15 | 1.3203 | 83.975 | 66.234 | 87.447 | 6° | 0.02 | 0.00421 | 70% |
| 0.30 | 1.3856 | 90.546 | 71.328 | 98.830 | 6° | 0.02 | 0.00412 | 70% |
| 0.46 | 1.6724 | 139.128 | 64.560 | 107.971 | 6° | 0.03 | 0.01388 | 70% |
| 0.50 | 1.0411 | 86.274 | 63.597 | 66.208 | 2° | 0.01 | 0.00430 | 70% |

Table 7: Airfoil performance at different M_∞ for baseline airfoil.

| M_∞ | C_L | C_L/C_D | $(C_L/C_D)_c$ | $(C_L^2/C_D)_c$ | AoA |
|------------|--------|-----------|---------------|-----------------|-------|
| 0.15 | 1.0789 | 47.616 | 47.616 | 51.371 | 6° |
| 0.30 | 1.1268 | 51.383 | 51.383 | 57.897 | 6° |
| 0.46 | 0.7745 | 44.112 | 44.112 | 34.166 | 2° |
| 0.50 | 0.8072 | 47.693 | 47.693 | 38.499 | 2° |

Fig. 5 and Fig. 6 are plots for Table. 3, Table. 5, and Table. 7. Comparing the optimum efficiency point of the baseline airfoil and CFJ airfoil, the CFJ airfoil improves the lift coefficient and aerodynamic efficiency by 60% or more under 100% pump efficiency. With a realistic CFJ pumping efficiency, the corrected aerodynamic efficiency is dropped, but still higher than the baseline by about 38%.

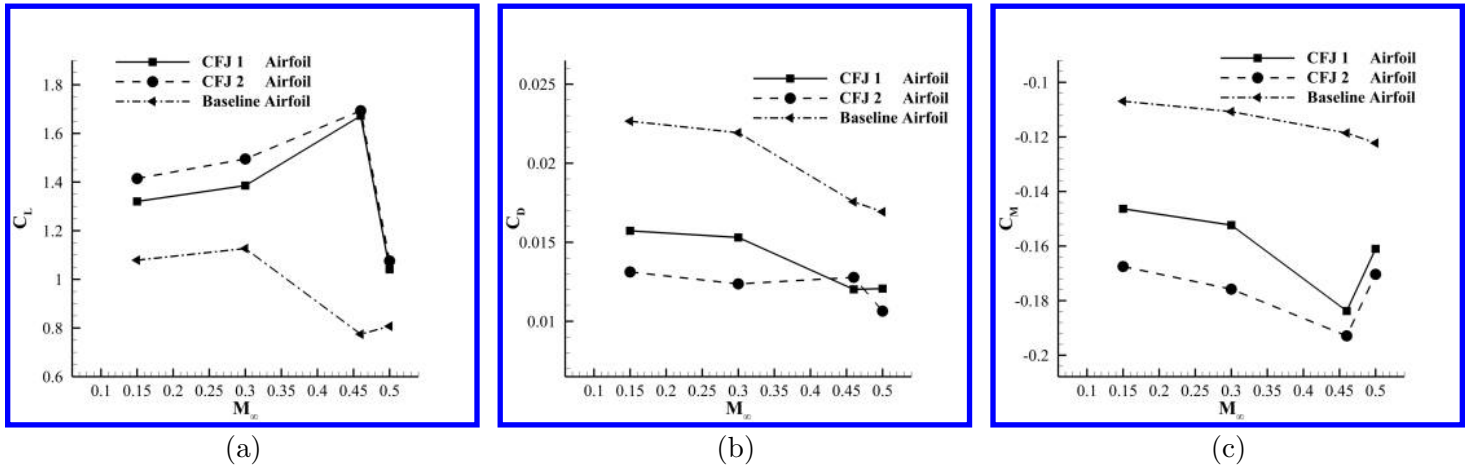


Figure 5: Lift, drag and moment coefficients for CFJ 1, CFJ 2, and baseline airfoils at their optimum aerodynamic efficiency.

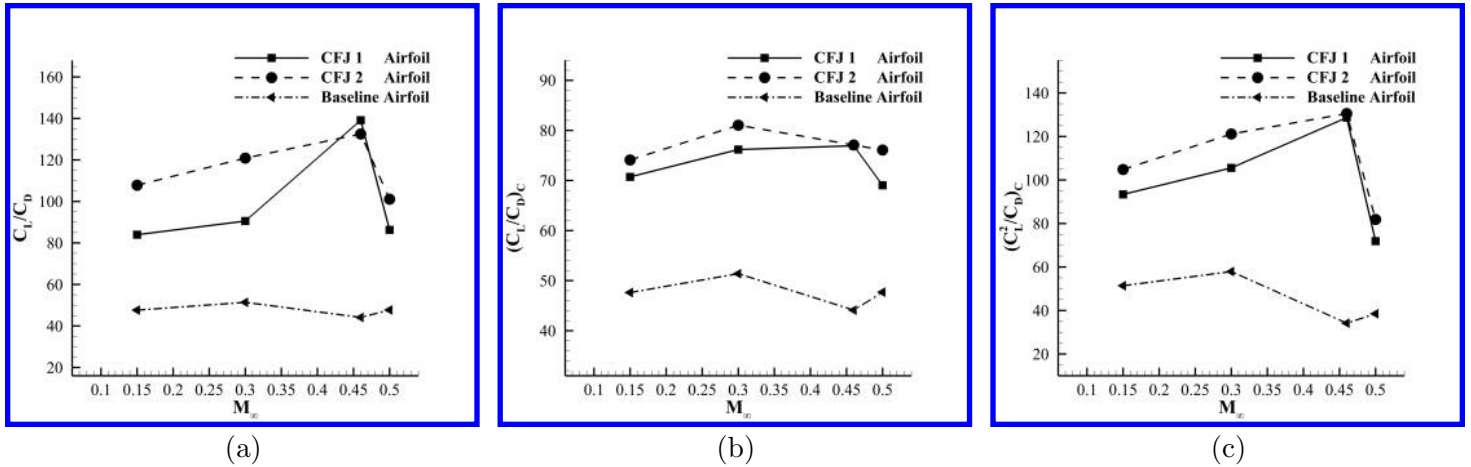


Figure 6: C_L/C_D , $(C_L/C_D)_c$, $(C_L^2/C_D)_c$ plots for CFJ 1, CFJ 2, and baseline airfoils at their optimum aerodynamic efficiency.

5.1 Performance of Different Airfoils under Constant C_μ

Since CFJ 2 airfoil performs better than the CFJ 1 airfoil, it is the focus of the present study. As shown in Table. 3, the CFJ 2 airfoil achieve the optimum efficiency mostly at C_μ of 0.03 and AoA of 6° except at M_∞ of 0.50. Hence the results to be presented have the C_μ of 0.03 for all the Mach numbers. For M_∞ of 0.50, the results of $C_\mu = 0.01$ is also added because it is the optimum.

Fig. 7 shows the Mach contours for all the cases with peak $(C_L/C_D)_c$ at different freestream Mach number. At Mach of 0.15, the flow is still in the incompressible flow regime with the peak Mach number less than 0.3. The maximum $(C_L/C_D)_c$ occurs at freestream Mach number of 0.3. This is because that the flow field is in the compressible flow regime with the peak Mach number of 0.54, but still far from transonic regime with no risk of shock waves. The compressible flow maximize the leading edge suction effect to enhance both the lift and reduce the drag at a low energy expenditure. When the freestream Mach number reaches 0.46, it is the critical Mach number for the airfoil. The maximum Mach number reaches 1, but no shock wave appears and hence the corrected aerodynamic efficiency is still very high with a value of 77 at the same AoA as at the lower Mach number. When the freestream Mach number reaches 0.5, the flow reaches transonic regime and a normal shock appears. The aerodynamic efficiency reduces to 69 at the same AoA . For M_∞ of 0.5, the peak aerodynamic efficiency condition of 76 is shifted to a lower AoA of 2° and the C_μ is decreased to 0.01. The lower AoA and C_μ remove the shock wave as shown in Fig. 8. The maximum Mach number on the CFJ airfoil suction surface reduces to 0.971 to keep the flow field to be subsonic.

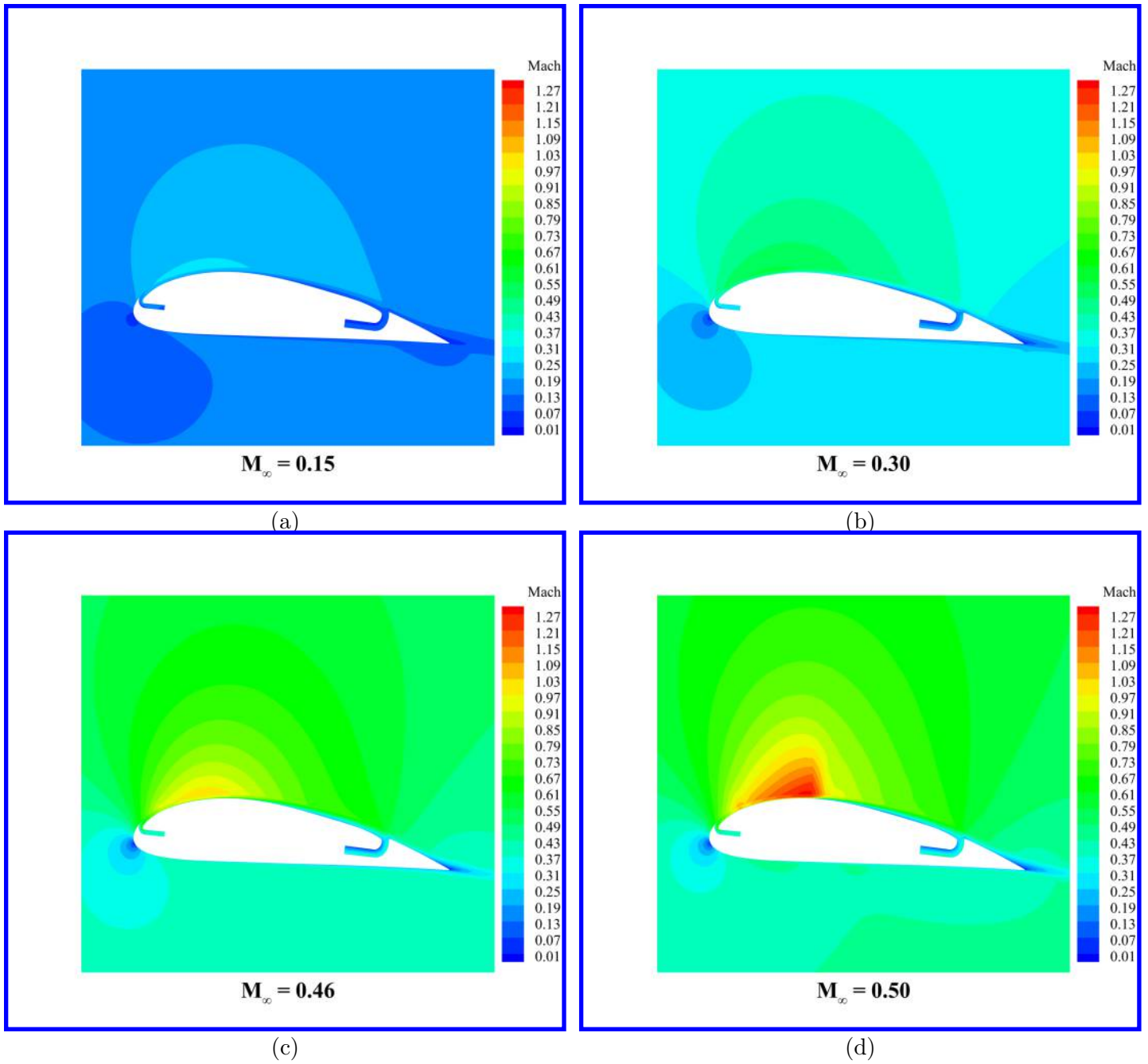


Figure 7: Mach contours for CFJ 2 airfoil at M_∞ of 0.15, 0.30, 0.46 and 0.50.

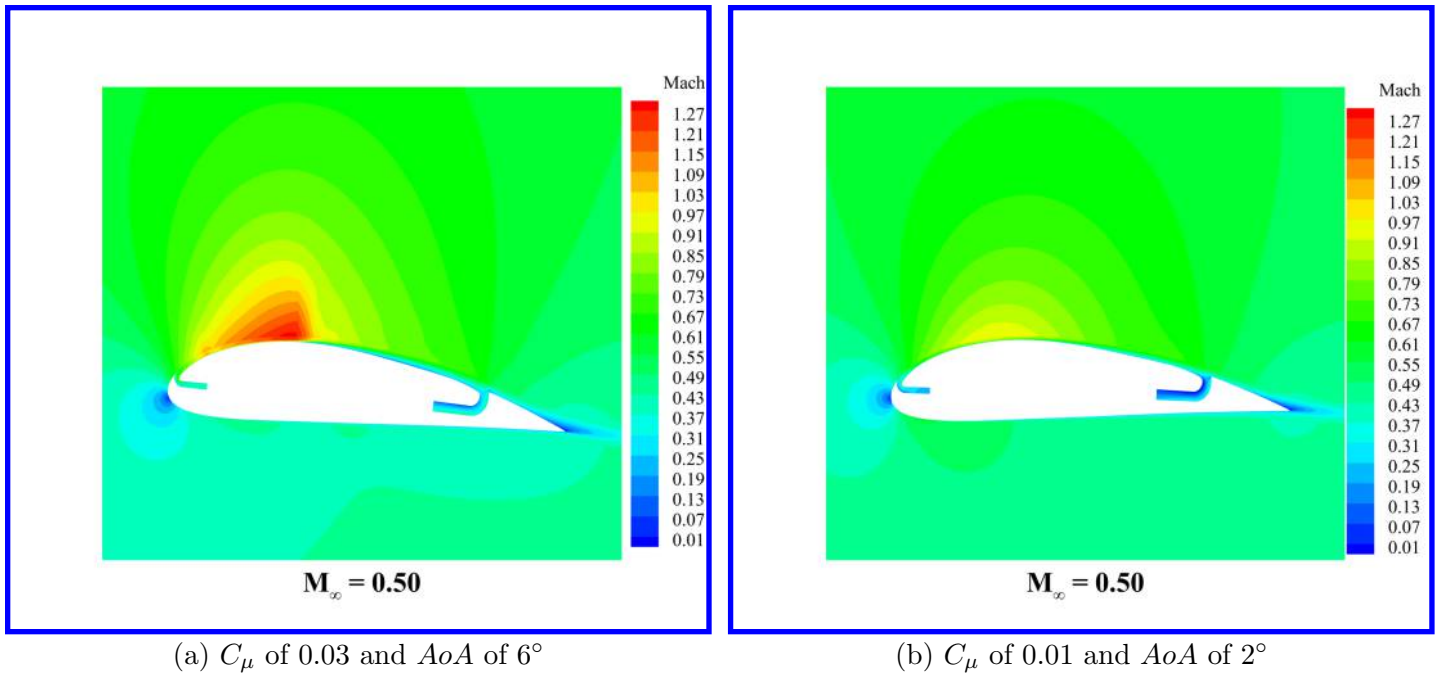


Figure 8: Mach contours for CFJ 2 airfoil at M_∞ of 0.50 with different C_μ and AoA .

The Lift, drag and moment coefficients vs. AoA for the CFJ airfoil are shown in Fig. 9. As the M_∞ increases, C_L also increases significantly due to the compressible flow effect. However, the drag coefficient C_D almost remains the same as shown in Fig. 9 (b). The nose down moment (C_M) is increased with the C_L .

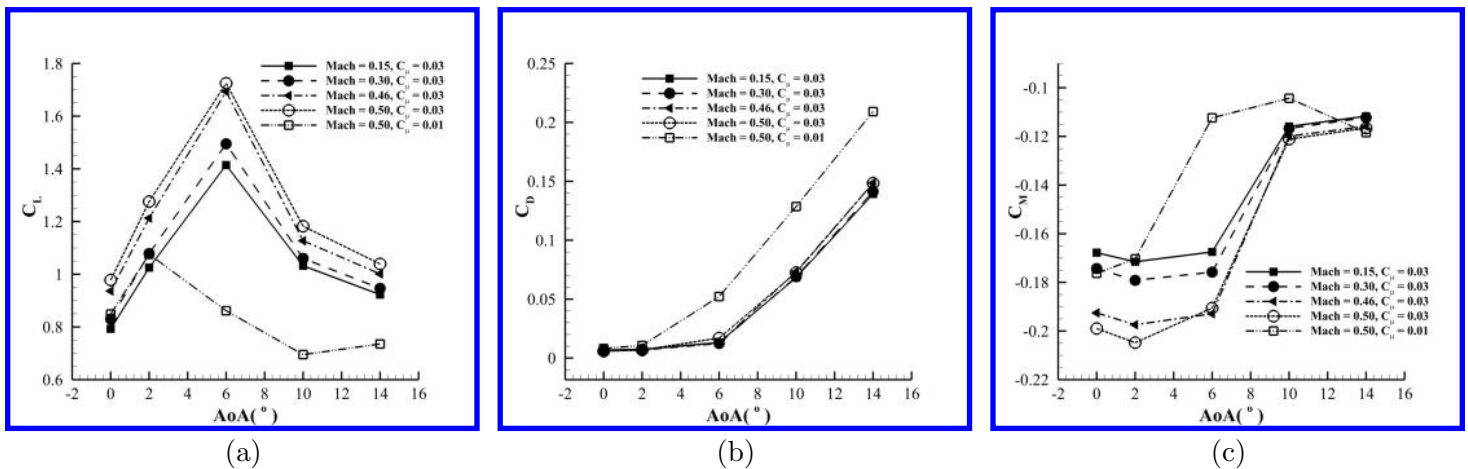


Figure 9: Lift, drag and moment coefficients for CFJ 2 airfoil.

Fig. 10 and Fig. 11 are plotted to compare the performance of CFJ 1 and NACA 6421 airfoils with CFJ 2 airfoil. Fig. 10 shows the lift, drag and moment coefficients for CFJ 1 airfoil at C_μ of 0.03. Fig. 11 shows the lift, drag and moment coefficients for NACA 6421 baseline airfoil which has no C_μ .

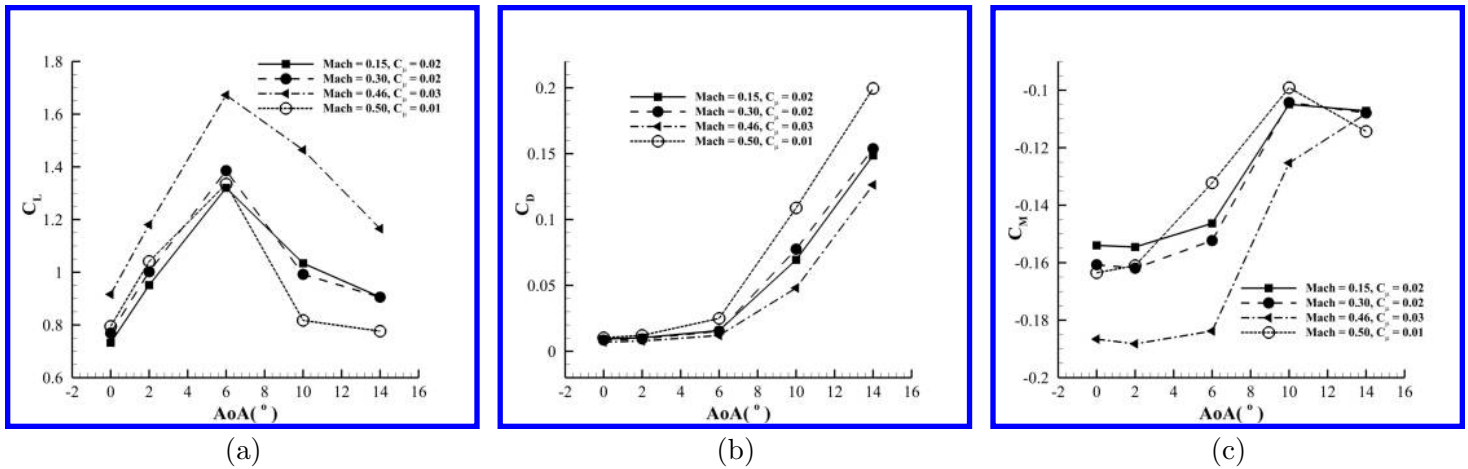


Figure 10: Lift, drag and moment coefficients for CFJ 1 airfoil at optimum C_{μ} .

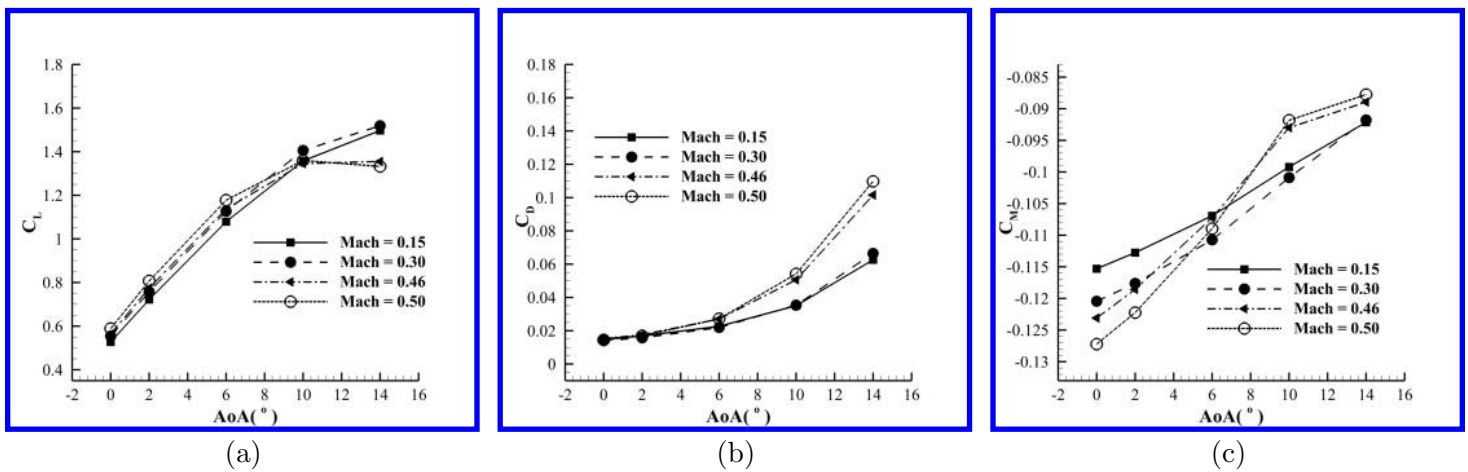


Figure 11: Lift, drag and moment coefficients for NACA 6421 airfoil.

The C_L/C_D , $(C_L/C_D)_c$, $(C_L^2/C_D)_c$ at different Mach number for the CFJ airfoil are shown in Fig. 12. As shown in Fig. 12 (a), all the peak C_L/C_D occurs at AoA of 2° . However, the peak $(C_L/C_D)_c$ occurs at AoA of 6° since the lift coefficient is the maximum and the power coefficient is the minimum. The productivity efficiency of $(C_L^2/C_D)_c$ has the similar trend to $(C_L/C_D)_c$.

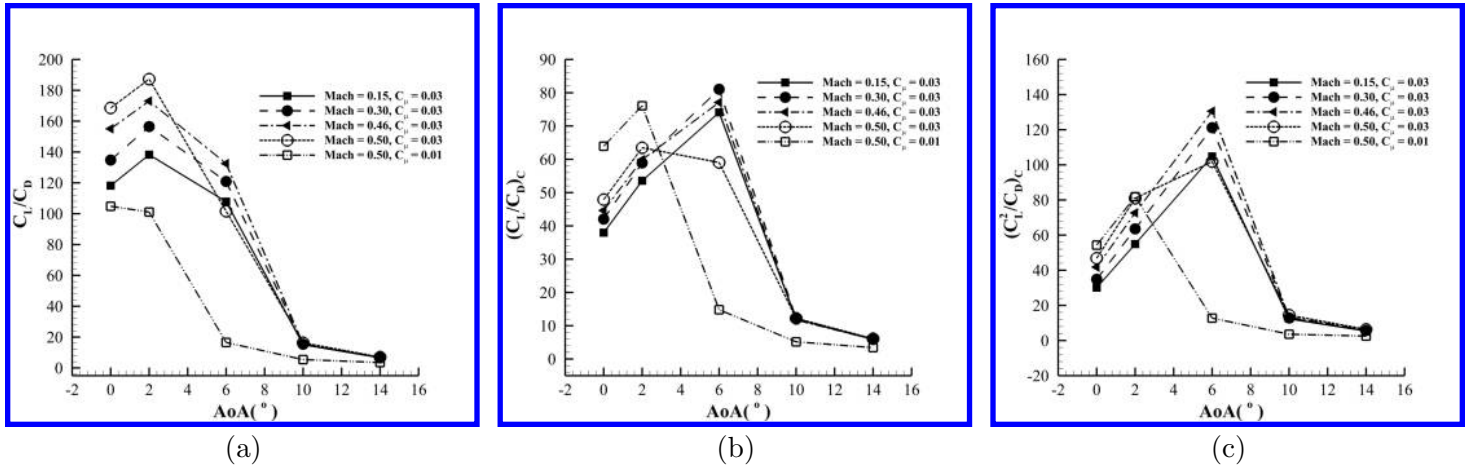


Figure 12: C_L/C_D , $(C_L/C_D)_c$, $(C_L^2/C_D)_c$ plots for CFJ 2 airfoil.

Fig. 13 and Fig. 14 are plotted to compare the performance of CFJ 1 and NACA 6421 airfoils with CFJ 2 airfoil. Fig. 13 shows the lift to drag ratio, aerodynamic efficiency, and productivity efficiency for CFJ 1 airfoil at C_{μ} of 0.03. Fig. 14 shows the lift to drag ratio, aerodynamic efficiency, and productivity efficiency for NACA 6421 baseline airfoil which has no C_{μ} and P_c , so that Fig. 14 (a) and Fig. 14 (b) are same.

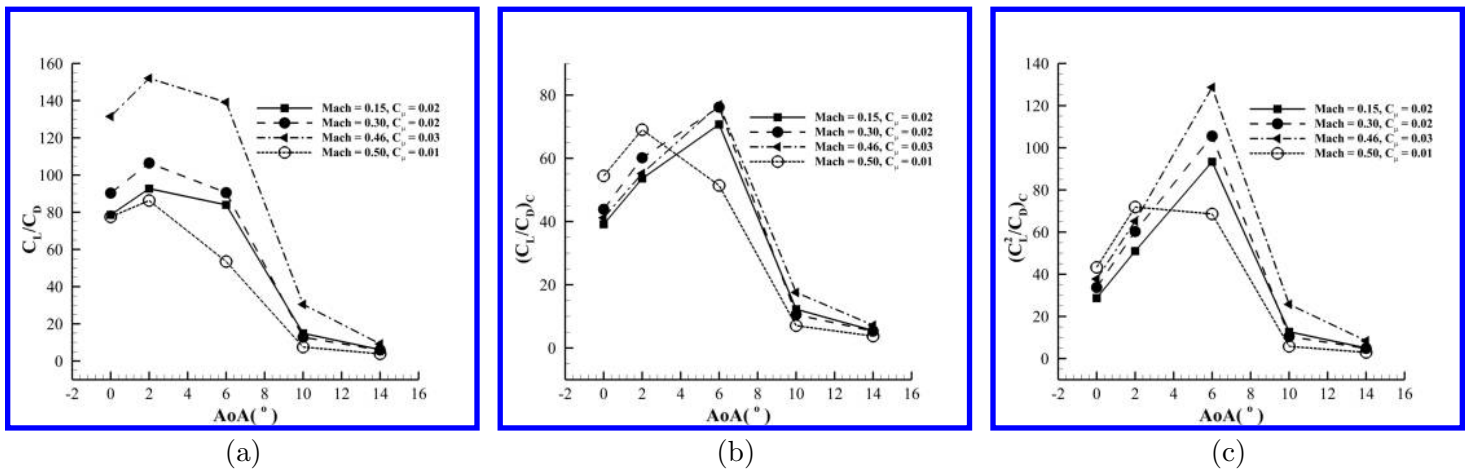


Figure 13: C_L/C_D , $(C_L/C_D)_c$, $(C_L^2/C_D)_c$ plots for CFJ 1 airfoil at optimum C_{μ} .

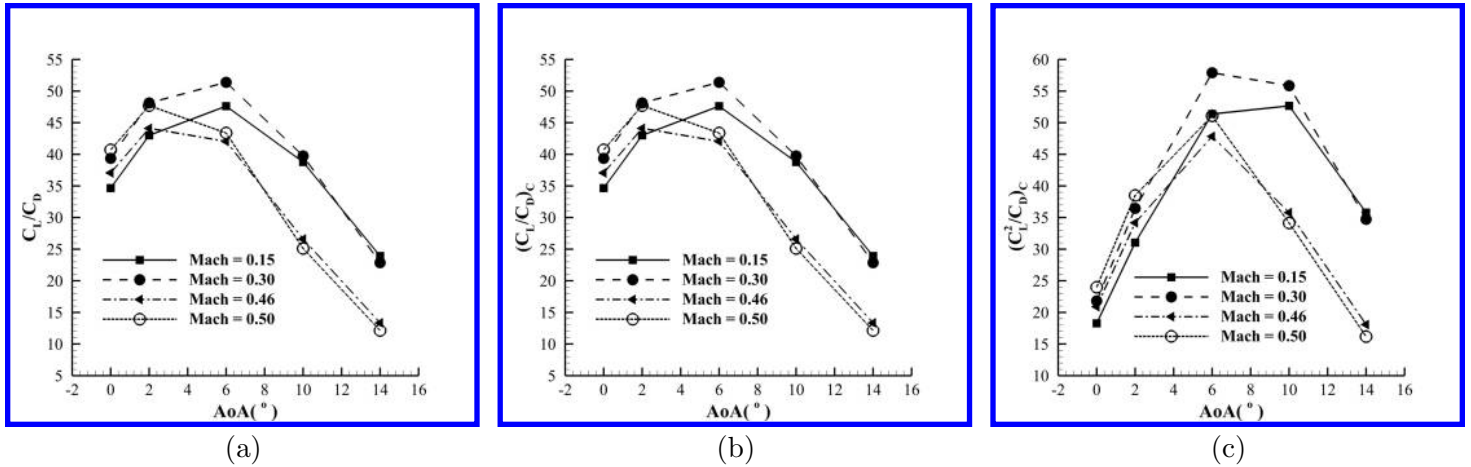


Figure 14: C_L/C_D , $(C_L/C_D)_c$, $(C_L^2/C_D)_c$ plots for NACA 6421 airfoil.

The power coefficient P_c and Isentropic Mach Number plots for the CFJ and baseline airfoil is shown in Fig. 15. M_∞ of 0.15 and M_∞ of 0.30 have the similar P_c since the maximum velocities are still at subsonic range. M_∞ of 0.46 and M_∞ of 0.50 have an increased P_c since the maximum Mach number reaches sonic and supersonic and the boundary layer loss is higher. A higher maximum Mach number gives a larger compressible flow effect with increased lift coefficient. However, once the maximum Mach number is supersonic, the efficiency will be affected due to increased entropy of shock wave.

As shown in Fig. 15 (b), as the freestream M_∞ increases, the loading becomes larger. The maximum Mach number on the airfoil for freestream Mach number (M_∞) of 0.15, 0.30, 0.46, 0.50 reaches 0.264, 0.558, 1.025 and 1.289 respectively. As long as the flows on the airfoil remains non-supersonic, the loading shapes are similar as shown in Fig. 15 (b). At M_∞ of 0.5, the flow on the airfoil becomes supersonic. A normal shock occurs at about 35% chord location. This thick airfoil modified from NACA 6421 for CFJ is not expected to work efficiently at transonic regime as a supercritical airfoil.

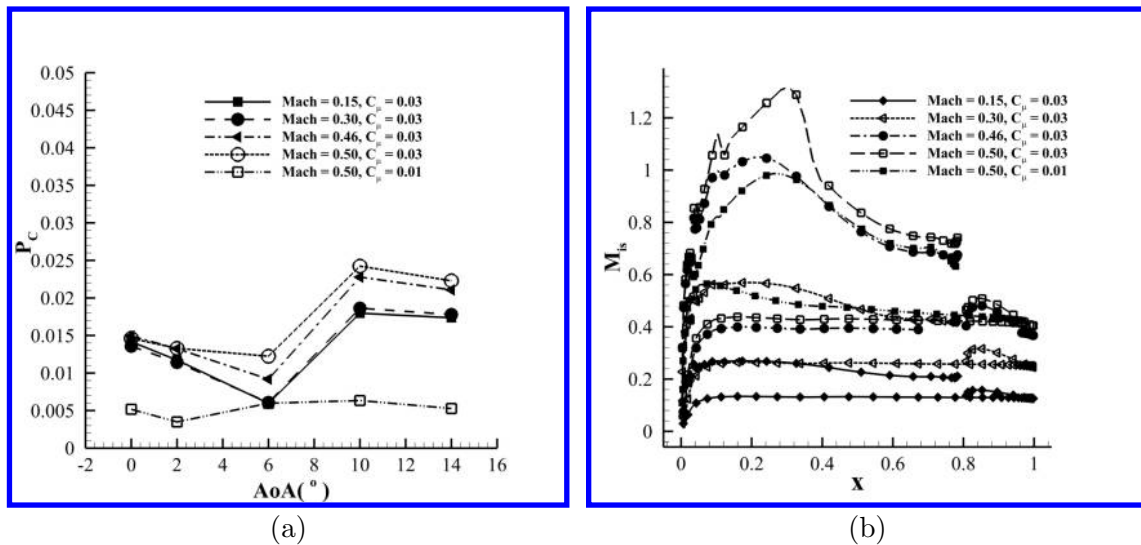


Figure 15: P_c and Isentropic Mach Number plots for CFJ 2 airfoil.

Fig. 16 is plotted in same scale with Fig. 15 to compare the aerodynamic performance between CFJ 1 and CFJ 2 airfoil. Since NACA 6421 airfoil does not have power consumption, it is not plotted. As we can see from Fig. 16 (a), the power consumption for CFJ 2 airfoil is smaller than that of CFJ 1 airfoil because of the enlarged injection slot. Fig. 17 shows the Isentropic Mach number plot for NACA 6421 baseline airfoil, which also has the same scale with Fig. 15 (b) and Fig. 16 (b). The Isentropic Mach number for NACA 6421 baseline airfoil is less than that of CFJ 1 and CFJ 2 airfoil at same freestream Mach number. Since there is no P_c involved in NACA 6421 baseline airfoil, thus there is no P_c plot for NACA 6421 baseline airfoil.

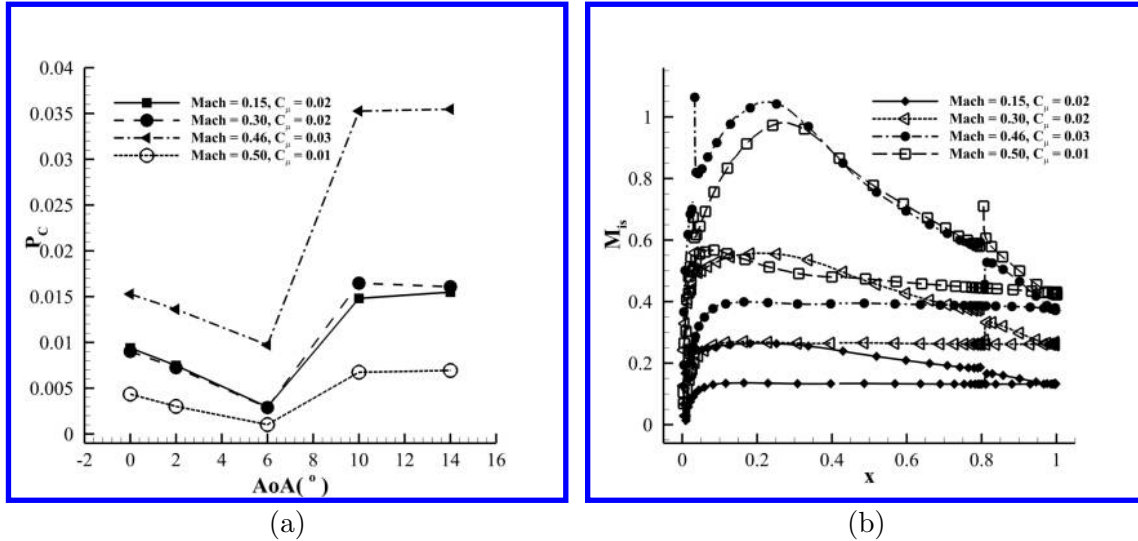


Figure 16: P_c and Isentropic Mach Number plots for CFJ 1 airfoil at optimum C_{μ} .

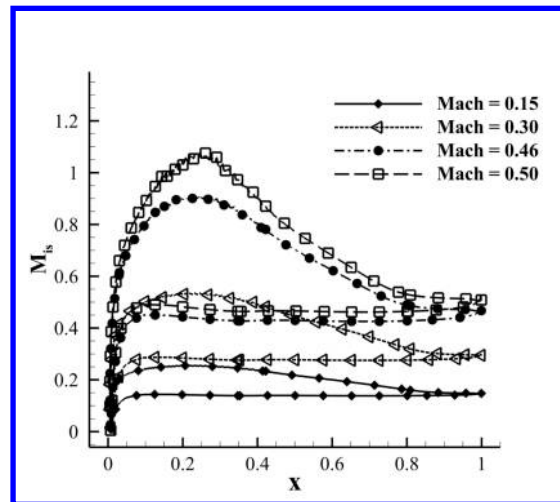


Figure 17: Isentropic Mach Number plots for NACA 6421 airfoil.

Fig. 18 (a) and (b) are the normalized injection total pressure and suction static pressure. The pressure is normalized as:

$$\bar{p} = p/(\rho_{\infty} V_{\infty}^2) \quad (11)$$

Fig. 18 (a) indicates that to achieve the same injection momentum coefficient, the injection total pressure is decreased with the increasing Mach number. This is because the leading edge suction effect is higher and the main flow pressure is lower in that region. Since the overall pressure level is lower with increased Mach number, the suction static pressure is also reduced. However, the more important parameter determining the power consumption is the total pressure ratio between the injection and suction slot as shown in Fig. 18 (b). For cruise Mach number at 0.15 and AoA of 6° , the total pressure ratio is at the level of 1.02. For Mach number of 0.3 and 0.46, it is increased to 1.08 and 1.2 respectively. For the cruise Mach number of 0.5 at AoA of 2° , the total pressure ratio is about 1.24. The required CFJ total pressure ratio is increased with increasing Mach number due to the boundary layer suffering more loss at higher speed. Fig. 19 (b) shows the mass averaged injection jet speed normalized by the freestream speed. The normalized jet speed is increased with the Mach number from 1.14 at Mach 0.15 to 1.24 at Mach 0.46. At cruise Mach number of 0.5, the optimum AoA is 2° , which requires a jet speed ratio of 1.155. Overall, the jet speed ratio is low and is beneficial for the low power required at cruise and the high efficiency shown in Fig. 12.

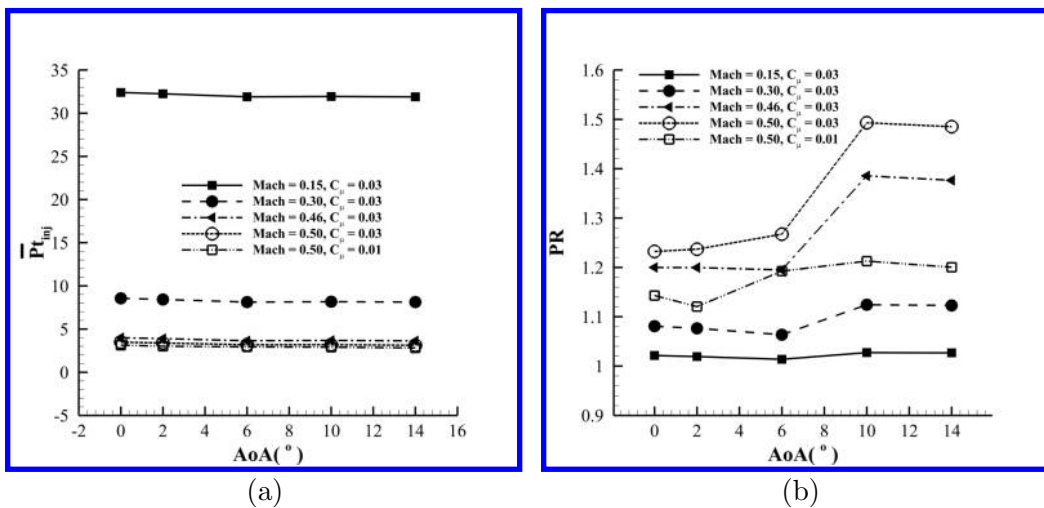


Figure 18: Injection total pressure and the total pressure ratio between injection and suction plots for CFJ 2 airfoil.

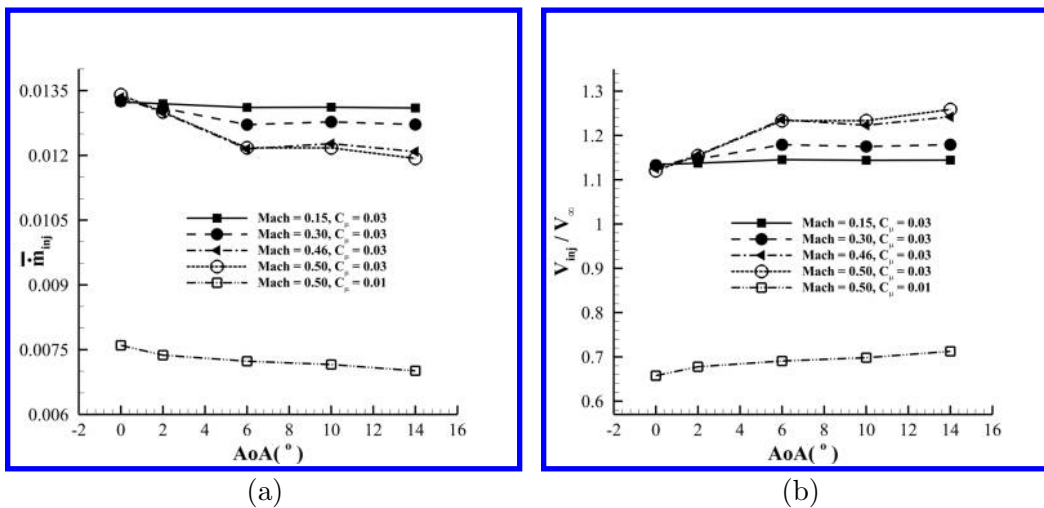


Figure 19: Normalized mass flow rate and injection velocity plots for CFJ 2 airfoil.

Fig. 20 and Fig. 21 are plotted for CFJ 1 airfoil to compare with CFJ 2 airfoil. The total pressure ratio between injection and suction are higher for CFJ 1 airfoil. The normalized mass flow rate for CFJ 1 airfoil is lower than that of CFJ 2 airfoil as shown in Fig. 20 (b). The injection velocity for CFJ 1 airfoil is higher than that of CFJ 2 airfoil as shown in Fig. 21 (b). Similarly, since NACA 6421 baseline airfoil has no CFJ system, there are no plots of injection total pressure, total pressure ratio between injection and suction, normalized mass flow rate, and normalized injection velocity.

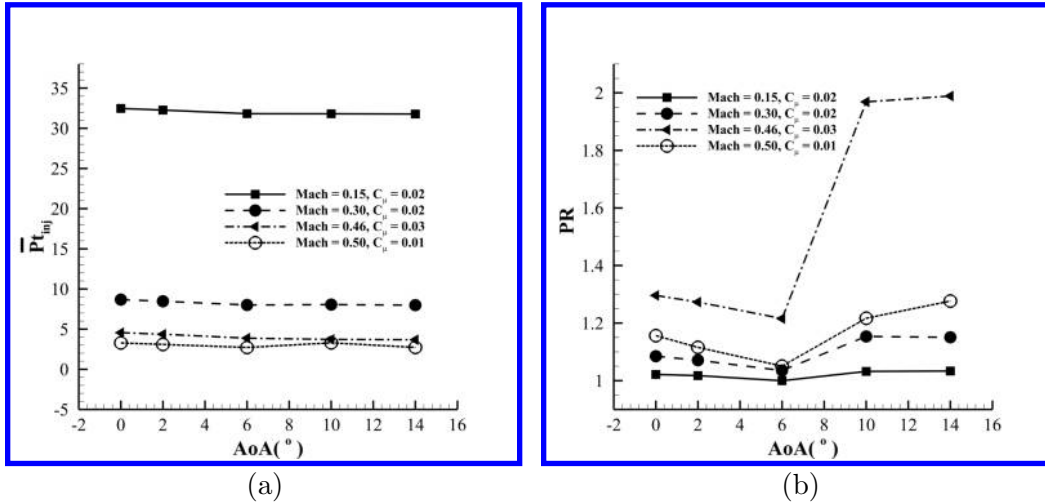


Figure 20: Injection total pressure and the total pressure ratio between injection and suction plots for CFJ 1 airfoil at optimum C_{μ} .

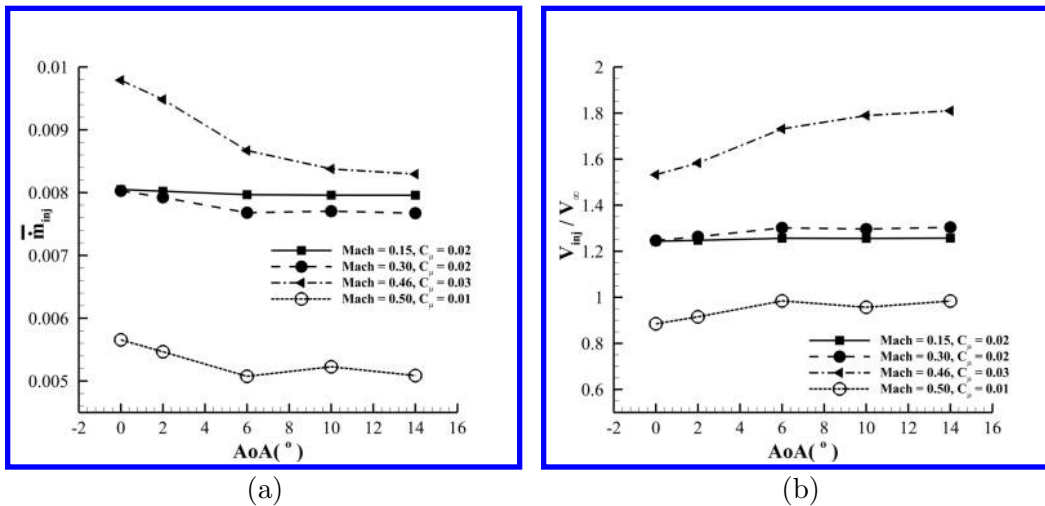


Figure 21: Normalized mass flow rate and injection velocity plots for CFJ 1 airfoil at optimum C_{μ} .

6 Fixed Injection Total Pressure

At cruise flight, when the AoA varies, it is easier to hold the injection total pressure constant as the control law for the micro-compressor. This section hence simulates the CFJ airfoil performance at cruise condition with the

injection total pressure held as constant. The total pressure value fixed is the one at the optimum aerodynamic efficiency point shown in Table. 3. For the freestream Mach number of 0.15, 0.3 and 0.46, the AoA is at 6° and C_μ is at 0.03. For the M_∞ of 0.5, the injection total pressure fixed is at AoA of 2° and C_μ of 0.01.

The P_c and C_μ plots for the CFJ airfoil at the fixed injection total pressure are shown in Fig. 22. Different from the constant C_μ cases shown in Fig. 15, both the P_c and C_μ have very low value at low AoA and are linearly increased with the AoA until the airfoil is stalled. These trends are the same as observed in the experiment[4, 3]. The low P_c at low AoA is because the flow is benign and the total pressure loss is low at the suction slot. At the same time the leading suction pressure on the suction surface is higher than at a greater AoA , the constant total pressure at the injection will generate lower jet velocity and smaller mass flow rate, which yields a lower injection momentum coefficient. With the AoA increasing, the pressure at the suction peak of the airfoil decreases, and the C_μ is increased. When the airfoil is stalled, the airfoil can not hold the low suction peak pressure and the C_μ drops.

There are two reasons that the power coefficient P_c is increased with the AoA when the injection total pressure is held as constant. First, the mass flow rate is increased due to the leading edge suction pressure decrease. The increased mass flow increases the power coefficient as shown in Eq. (7) and Eq. (8). Second, the total pressure ratio loss is increased when the AoA is increased since the injection velocity is higher and the boundary layer goes through more diffusion before going into the suction duct. With a lower suction total pressure, the pressure ratio is higher to reach the same injection total pressure, the power coefficient is thus increased.

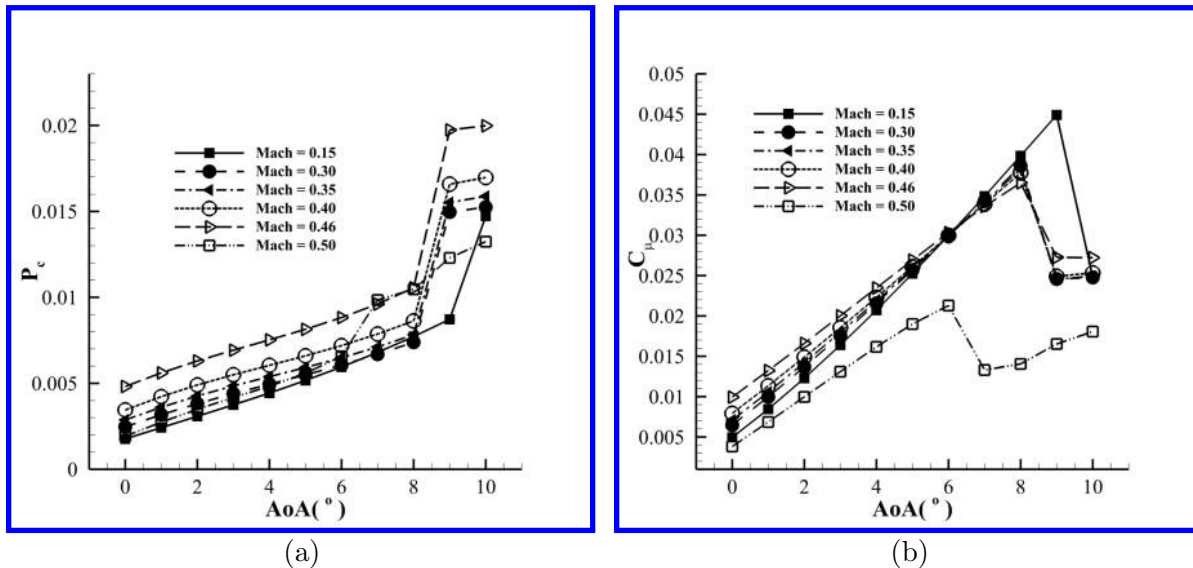


Figure 22: P_c and C_μ plots for CFJ airfoil at different Mach number.

As shown in Fig. 23 (a), after AoA of 4° , the injection mass flow rate normalized by its corresponding freestream conditions is higher at lower Mach number. Note that the actual injection mass flow rate is higher with the increased freestream Mach number. As shown in Fig. 23 (b), the higher Mach number gives higher injection velocity normalized by the freestream velocity. The injection velocity also increases with the increasing AoA due to the decreased leading edge suction peak pressure.

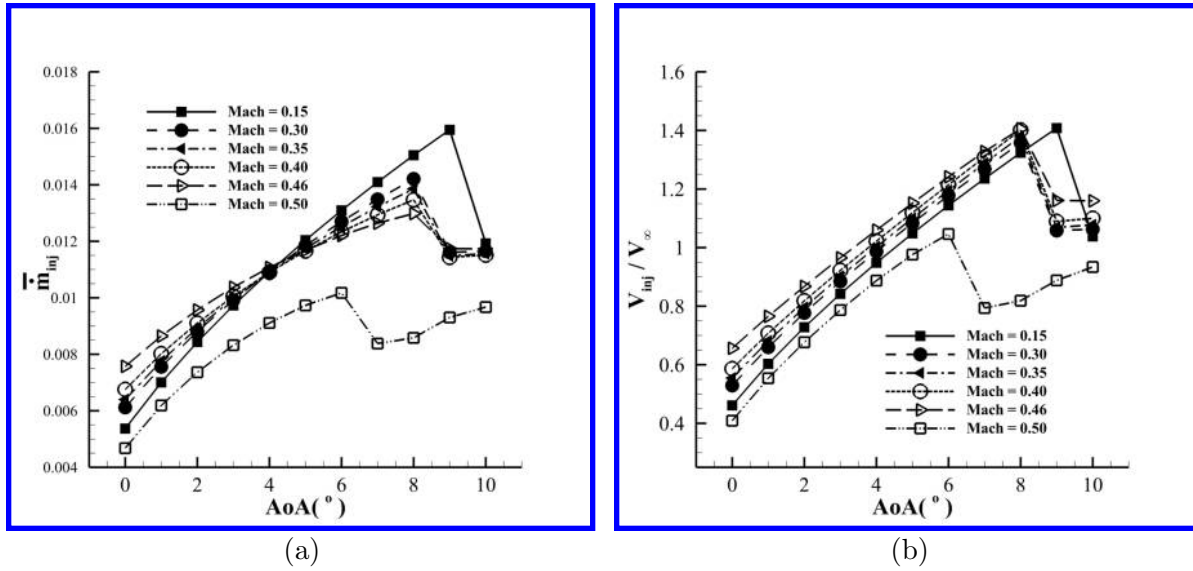


Figure 23: m_{inj} and V_{inj} plots for CFJ airfoil at different Mach number.

The Lift, drag and moment coefficient vs. AoA for the CFJ airfoil at a fixed injection total pressure at different Mach number are shown in Fig. 24. As the M_{∞} increases, C_L also increases significantly due to the compressibility effect. However, the drag coefficient C_D almost remains the same as shown in Fig. 24 (b). Since the total pressure is fixed, which allows C_{μ} varies by its iterations. The stall AoA is about 8° , except for Mach number of 0.15, which is at 9° as shown in Fig. 24 (a). For a fixed C_{μ} , the nose down moment (C_M) is increased until the stall AoA is approached as shown in Fig. 24 (c).

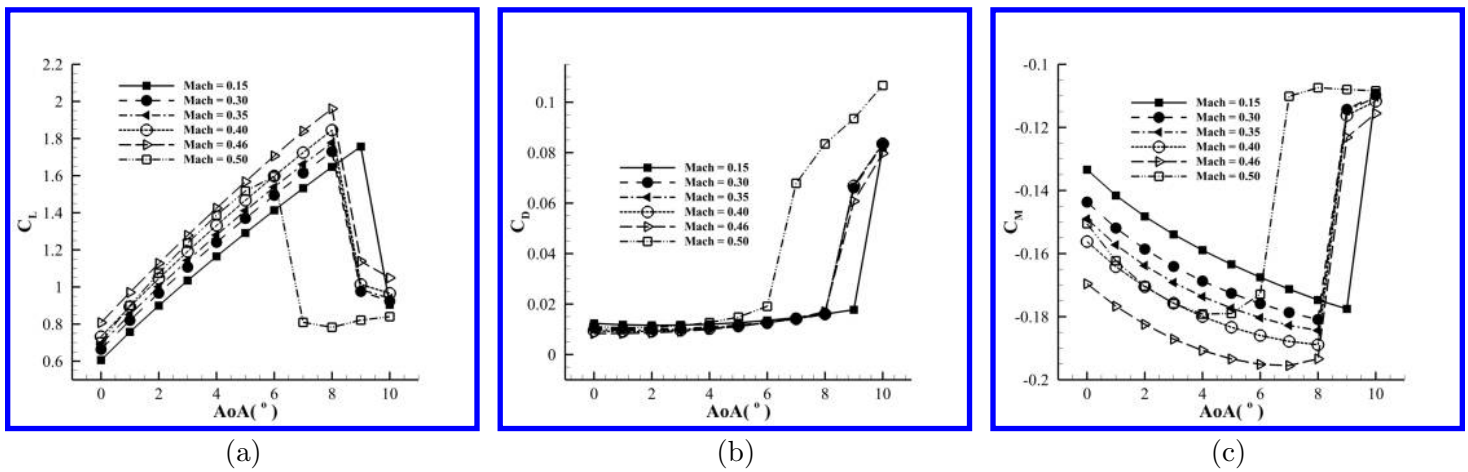


Figure 24: Lift, drag and moment coefficients for CFJ airfoil at different Mach number.

The C_L/C_D , $(C_L/C_D)_c$, $(C_L^2/C_D)_c$ for a fixed injection total pressure at different Mach number for the CFJ airfoil are shown in Fig. 25. As shown in Fig. 25 (a), all the peak C_L/C_D occurs at AoA of 4° . However, the peak $(C_L/C_D)_c$ occurs at AoA of 6° as same as cases with fixed C_{μ} . The productivity efficiency has the peak value at 8° because the C_L keeps increasing until it stalls.

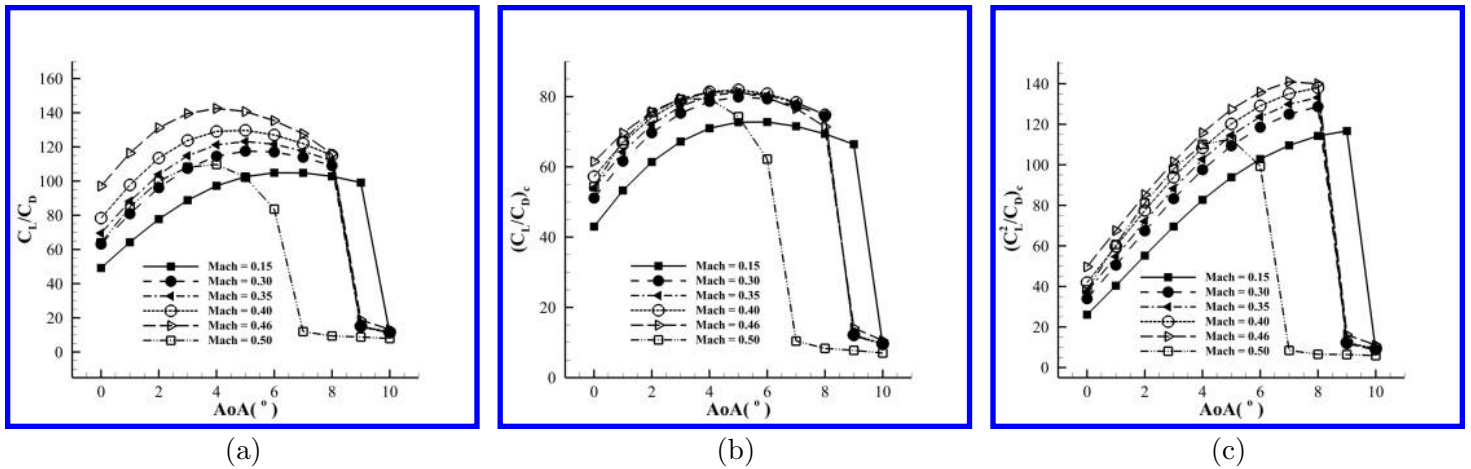


Figure 25: C_L/C_D , $(C_L/C_D)_c$, $(C_L^2/C_D)_c$ plots for CFJ airfoil at different Mach number.

Fig. 26 shows the injection total pressure versus the freestream Mach number. Overall, the injection total pressure is decreased with the increasing freestream Mach number because the static pressure is lower at the leading edge suction peak when the freestream Mach number is increased.

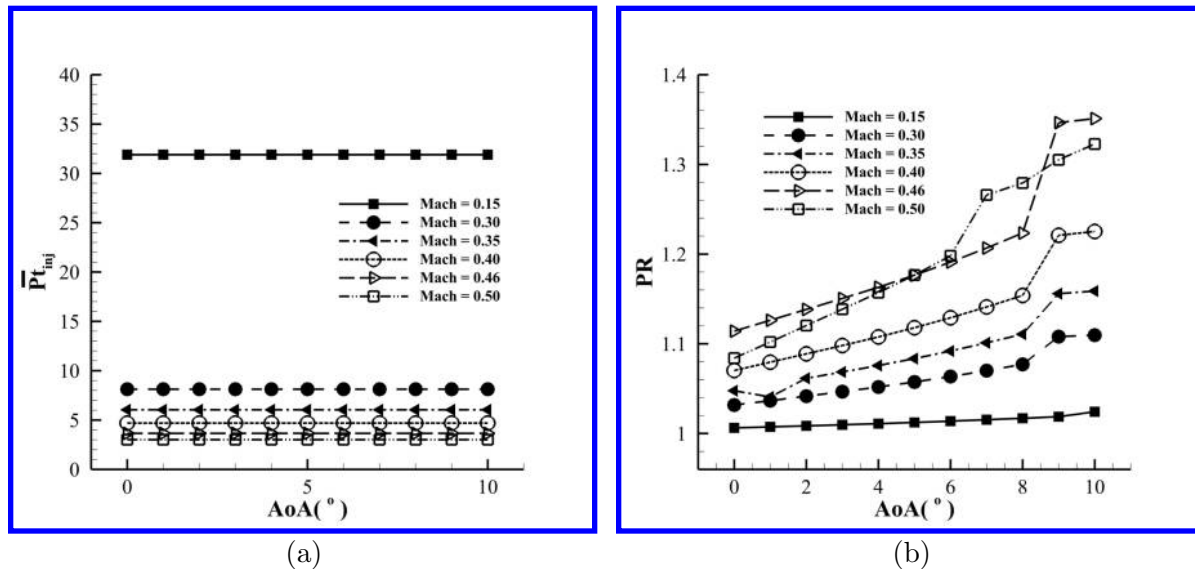


Figure 26: P_t and PR plots for CFJ airfoil at different Mach number.

7 Conclusion

This paper compares the aerodynamic performance, energy expenditure, and 2D flow field at cruise conditions with different freestream M_∞ of 0.15, 0.30, 0.46, and 0.50 for the baseline NACA 6421 airfoil and two CFJ airfoil modified from the baseline airfoil, namely CFJ6421-SST150-SUC133-INJ065 airfoil (CFJ 1) and CFJ6421-SST150-SUC247-INJ117 airfoil (CFJ 2). The results show that the highest CFJ airfoil corrected efficiency ($(C_L/C_D)_c$) is at M_∞ 0.30, which gives $(C_L/C_D)_c$ of 81.04 at C_μ 0.03 and at AoA of 6° . At C_μ 0.03 and at AoA of 6° , the maximum velocity of M_∞ of 0.15, 0.30, 0.46, and 0.50 are Mach 0.264, 0.558, 1.025 and 1.289 respectively. Since

the flow becomes transonic at M_∞ of 0.50, the optimum cruise $(C_L/C_D)_c$ for M_∞ of 0.5 occurs at AoA of 2° and C_μ of 0.01 with the maximum Mach number dropped to 0.971.

Both the CFJ airfoils increase the aerodynamic efficiency by over 50% compared with the baseline NACA 6421 airfoil. At the same time, the cruise lift coefficient is also increased substantially. As the result, the productivity efficiency is increased up to 100%. Between the two CFJ airfoils, the CFJ 2 airfoil with the injection slot enlarged by 80% is a little better than the CFJ 1 airfoil because the larger slot has lower jet velocity and CFJ pressure ratio. The advantage of the CFJ 2 airfoil with the larger injection slot is more significant than the CFJ 1 airfoil at VTOL or ESTOL when a super-lift coefficient is required, because the required CFJ power is substantially reduced [27]. For the optimum cruise condition with the Mach number varying from 0.15 to 0.5, the injection jet velocity ratio is varied from 1.24 to 0.68, and the total pressure ratio between the injection and suction slot is from 1.02 to 1.20. The low jet velocity is beneficial to reduce the noise and the low total pressure ratio is beneficial to achieve the low power requirement at cruise.

This paper also studies two control laws at cruise when the AoA varies: 1) constant injection jet momentum coefficient C_μ ; 2) Constant injection jet total pressure, Pt_{inj} holding the value of the optimum injection total pressure from the cases of constant C_μ . Holding the injection total pressure constant may be a more suitable control law for CFJ actuators because the total pressure is easier to measure. The CFJ airfoil performance trend is different with constant C_μ and constant Pt_{inj} . For constant C_μ , the CFJ power coefficient is decreased when the AoA increases until the airfoil is near stalled due to the lower leading edge suction effect. For the constant Pt_{inj} , the power coefficient and C_μ increase with increasing AoA . The important advantages of the constant Pt_{inj} over constant C_μ are: 1) It has higher aerodynamic and productivity efficiency at low AoA . 2) It has higher stall AoA . These features are very beneficial to expand the flight envelop with higher cruise efficiency and reliability.

8 Acknowledgment

The simulations are conducted on Pegasus super computing system at the Center for Computational Sciences at the University of Miami.

References

- [1] G.-C. Zha and D. C. Paxton, "A Novel Flow Control Method for Airfoil Performance Enhancement Using Co-Flow Jet." *Applications of Circulation Control Technologies*, Chapter 10, p. 293-314, Vol. 214, Progress in Astronautics and Aeronautics, AIAA Book Series, Editors: Joslin, R. D. and Jones, G.S., 2006.
- [2] G.-C. Zha, W. Gao, and C. Paxton, "Jet Effects on Co-Flow Jet Airfoil Performance," *AIAA Journal*, No. 6, vol. 45, pp. 1222–1231, 2007.
- [3] G.-C. Zha, C. Paxton, A. Conley, A. Wells, and B. Carroll, "Effect of Injection Slot Size on High Performance Co-Flow Jet Airfoil," *AIAA Journal of Aircraft*, vol. 43, 2006.
- [4] G.-C. Zha, B. Carroll, C. Paxton, A. Conley, and A. Wells, "High Performance Airfoil with Co-Flow Jet Flow Control," *AIAA Journal*, vol. 45, 2007.
- [5] Wang, B.-Y. and Haddoukessouni, B. and Levy, J. and Zha, G.-C., "Numerical Investigations of Injection Slot Size Effect on the Performance of Co-Flow Jet Airfoil," *Journal of Aircraft*, vol. Vol. 45, No. 6, pp. pp.2084–2091, 2008.

- [6] B. P. E. Dano, D. Kirk, and G.-C. Zha, "Experimental Investigation of Jet Mixing Mechanism of Co-Flow Jet Airfoil." AIAA-2010-4421, 5th AIAA Flow Control Conference, Chicago, IL, 28 Jun - 1 Jul 2010.
- [7] B. P. E. Dano, G.-C. Zha, and M. Castillo, "Experimental Study of Co-Flow Jet Airfoil Performance Enhancement Using Micro Discreet Jets." AIAA Paper 2011-0941, 49th AIAA Aerospace Sciences Meeting, Orlando, FL, 4-7 January 2011.
- [8] A. Lefebvre, B. Dano, W. Bartow, M. Fronzo, and G. Zha, "Performance and energy expenditure of coflow jet airfoil with variation of mach number," *Journal of Aircraft*, vol. 53, no. 6, pp. 1757–1767, 2016.
- [9] A. Lefebvre, G.-C. Zha, "Numerical Simulation of Pitching Airfoil Performance Enhancement Using Co-Flow Jet Flow Control," *AIAA paper 2013-2517*, June 2013.
- [10] A. Lefebvre, G.-C. Zha, "Cow-Flow Jet Airfoil Trade Study Part I : Energy Consumption and Aerodynamic Performance," *32nd AIAA Applied Aerodynamics Conference, AIAA AVIATION Forum, AIAA 2014-2682*, June 2014.
- [11] A. Lefebvre, G.-C. Zha, "Cow-Flow Jet Airfoil Trade Study Part II : Moment and Drag," *32nd AIAA Applied Aerodynamics Conference, AIAA AVIATION Forum, AIAA 2014-2683*, June 2014.
- [12] Lefebvre, A. and Zha, G.-C., "Trade Study of 3D Co-Flow Jet Wing for Cruise Performance." AIAA Paper 2016-0570, AIAA SCITECH2016, AIAA Aerospace Science Meeting, San Diego, CA, 4-8 January 2016.
- [13] Lefebvre, A. and Zha, G.-C. , "Design of High Wing Loading Compact Electric Airplane Utilizing Co-Flow Jet Flow Control." AIAA Paper 2015-0772, AIAA SciTech2015: 53rd Aerospace Sciences Meeting, Kissimmee, FL, 5-9 Jan 2015.
- [14] Liu, Z.-X. and Zha, G.-C., "Transonic Airfoil Performance Enhancement Using Co-Flow Jet Active Flow Control." AIAA Paper 2016-3066, AIAA Aviation, June 13-17 2016.
- [15] Yunchao Yang and Gecheng Zha, "Super-Lift Coefficient of Active Flow Control Airfoil: What is the Limit?." AIAA Paper 2017-1693, AIAA SCITECH2017, 55th AIAA Aerospace Science Meeting, Grapevine, January 9-13 2017.
- [16] Lefebvre, A. and Dano, B. and Bartow, W. and Di Franzo, M. and Zha, G.-C., "Performance Enhancement and Energy Expenditure of Co-Flow Jet Airfoil with Variation of Mach Number." AIAA Paper 2013-0490, AIAA Journal of Aircraft, DOI: 10.2514/1.C033113, 2016.
- [17] P. R. Spalart and S. R. Allmaras, "A one-equation turbulence model for aerodynamic flows," in *30th Aerospace Sciences Meeting and Exhibit, Aerospace Sciences Meetings, Reno, NV, USA, AIAA Paper 92-0439*, 1992.
- [18] Y.-Q. Shen and G.-C. Zha, "Large Eddy Simulation Using a New Set of Sixth Order Schemes for Compressible Viscous Terms ," *Journal of Computational Physics*, vol. 229, pp. 8296–8312, 2010.
- [19] Zha, G.C., Shen, Y.Q. and Wang, B.Y., "An improved low diffusion E-CUSP upwind scheme ," *Journal of Computer and Fluids*, vol. 48, pp. 214–220, Sep. 2011.
- [20] Y.-Q. Shen and G.-Z. Zha , "Generalized finite compact difference scheme for shock/complex flowfield interaction," *Journal of Computational Physics*, vol. doi:10.1016/j.jcp.2011.01.039, 2011.
- [21] Shen, Y.-Q. and Zha, G.-C. and Wang, B.-Y., "Improvement of Stability and Accuracy of Implicit WENO Scheme," *AIAA Journal*, vol. 47, No. 2, pp. 331–344, 2009.

- [22] Shen, Y.-Q. and Zha, G.-C. and Chen, X.-Y., “ High Order Conservative Differencing for Viscous Terms and the Application to Vortex-Induced Vibration Flows,” *Journal of Computational Physics*, vol. 228(2), pp. 8283–8300, 2009.
- [23] Shen, Y.-Q. and Zha, G.-C. , “ Improvement of the WENO Scheme Smoothness Estimator,” *International Journal for Numerical Methods in Fluids*, vol. DOI:10.1002/flid.2186, 2009.
- [24] G.-C. Zha and E. Bilgen, “Numerical Study of Three-Dimensional Transonic Flows Using Unfactored Upwind-Relaxation Sweeping Algorithm,” *Journal of Computational Physics*, vol. 125, pp. 425–433, 1996.
- [25] B.-Y. Wang and G.-C. Zha, “A General Sub-Domain Boundary Mapping Procedure For Structured Grid CFD Parallel Computation,” *AIAA Journal of Aerospace Computing, Information, and Communication*, vol. 5, No.11, pp. 2084–2091, 2008.
- [26] Y.-Q. Shen, G.-C. Zha, and B.-Y. Wang, “Improvement of Stability and Accuracy of Implicit WENO Scheme ,” *AIAA Journal*, vol. 47, pp. 331–344, 2009.
- [27] Wang, Yang. and Yang, Yunchao. and Zha, G.-C., “Study of Super-Lift Coefficient of Co-Flow Jet Airfoil and Its Power Consumption.” Proceeding AIAA Paper 2019, AIAA AVIATION Forum 2019, AIAA Aviation and Aeronautics Forum and Exposition, Dallas, Texas, June 17-21, 2019.